Shear flow in the infinite-shear-rate limit

István Borzsák and András Baranyai
Laboratory of Theoretical Chemistry, Eötvös University, Budapest 112, Pf. 32, 1518 Hungary
(Received 28 September 1994; revised manuscript received 16 March 1995)

Computer simulations have revealed the existence of a disorder-order phase transition in simple shearing liquids [J. J. Erpenbeck, Phys. Rev. Lett. **52**, 1333 (1984)]. Above a certain shear rate, the motion of the particles becomes ordered. This high-shear-rate structure, the so-called string phase, is studied numerically in order to investigate the possibility of such a transition taking place in real systems. At first we determined the optimal arrangements of spherical particles in the string phase. In the high-density infinite-shear-rate limit, where the random thermal motion of particles is negligible, minimum energy structures can be found as functions of density and interaction. We identify these structures and relate them to equilibrium ones. Utilizing the symmetry of the limit structure, we perform nonequilibrium molecular dynamics simulations at high but finite shear rates in order to study the coexistence conditions of liquid and string phases as a function of periodic boundary symmetry and system size. The stability of the string phase depends significantly on these aspects of the simulations. The larger the system, the less stable the pure string phase is compared to the coexisting liquid-string formation. This calls into question the existence of this phase transition in real shearing fluids. We also study the liquid-string transition in terms of the so-called phase space compressibility factor $\langle \Lambda \rangle$, since it was found recently [D. J. Evans and A. Baranyai, Phys. Rev. Lett. **67**, 2597 (1991)] that this simple phase variable exhibits a local extremum property even far from equilibrium. In the thermodynamic limit, $\langle \Lambda \rangle$ correctly estimates the shear rate at which the liquid phase becomes unstable in computer simulations.

PACS number(s): 64.70.Ja, 47.20.Ft, 61.20.Ja

I. INTRODUCTION

In computer simulations of nonequilibrium steady state (NESS) systems, it is mandatory to remove the dissipative heat produced by the external field (e.g., shear rate) in order to maintain the steady state. This can be done most efficiently by so-called synthetic thermostats which are included explicitly in the equations of motion [1]. These thermostats will not change the *linear* response of the system. Far from equilibrium, however, the thermostatting mechanism will influence the properties of the NESS system. Thus different thermostats might produce different properties for otherwise identical systems. For planar Couette flow, the simplest and most popular thermostats make the assumption that the streaming velocity profile of the liquid is linear [so-called profile biased thermostats (PBT's)]. This must clearly be true close to equilibrium. Away from equilibrium, however, kink instabilities might develop with the result that the assumption of a linear velocity profile cannot be maintained. In this case it is crucial to apply a thermostat which correctly takes into account the possibility of nonlinear flow profiles [profile unbiased thermostats (PUT's)] [1].

The paramount importance of correct thermostatting became evident when nonequilibrium molecular dynamics (NEMD) simulations revealed an interesting phase transition in shearing liquids [2]. If the shear rate was gradually increased, the amorphous liquid phase was observed to change its structure: the particles were found to organize themselves into *strings*. This new arrangement reduces the stress in the system. Since then the string phase has been the subject of disagreement in the literature [3]. The key question is whether this phase is a mere artifact of the computational method [4] or a structure having its counterpart in real systems [5]. Ackerson and Pusey have studied colloid suspensions, where they found evidence of shear-induced ordering upon application of an oscillatory field [6]. However, they did not find an ordering transition induced by steady shear.

Simultaneous efforts have been under way in model calculations. Evans and Morriss argued [1] that the ordered phase is merely the result of the PBT mechanism. It should be noted here that in simple model systems (containing Lennard-Jones particles) the string phase is formed under fairly extreme conditions. Since the pairwise additive, spherically symmetric Lennard-Jones potential is considered to be a reasonable approximation for the description of liquid argon, we can transform the shear rate value of this transition into real units. The shear rate γ necessary to turn a liquid into strings corresponds to $\gamma > 10^{12}$ Hz using the parameters of liquid argon. In fact, it has been demonstrated in a realistic NEMD simulation that this system is unable to remove the viscous heat towards the boundaries. For shear rates an order of magnitude smaller than the liquid-string transition value, the natural heat conductivity of the system is insufficient to maintain steady conditions and the liquid heats up [7].

The situation is somewhat different in charge-stabilized colloidal suspensions where the surrounding solvent molecules act as a fast and efficient heat bath for the colloidal particles. In this case, the existence of the liquid-string transition of shearing colloidal particles cannot be excluded for the reasons mentioned above. It still must be

decided, however, how the thermostat can be mimicked correctly in simulations where the solvent molecules are not modeled explicitly. Since it is not the purpose of this paper to elaborate on the proper synthetic thermostats for NESS systems, we simply report the observations that string phases have been produced with PBT [2,9] and layered PUT [5,8] thermostats but it has proved impossible with PUT's [1,4].

The purpose of the present paper is to study the possibility of this phase transition from another viewpoint. Structural transformations observed during computer simulations have very pronounced dependence on system size and symmetry constraints. The properties of this transition in terms of size and symmetry may shed some light on the whole problem. To our knowledge a study of this kind has not been performed to date.

Our first aim is to find the most stable structure of the string phase. Without a suitable thermodynamic theory, however, we have to restrict ourselves to the only well-defined state of the system, the infinite shear rate limit at high densities. The infinite-shear-rate limit is analogous to some extent to the limit of absolute zero temperature of equilibrium systems (crystalline solids), since the random thermal motion of the particles relative to their hydrodynamic speed is negligible at high densities. Since we know no practical way to determine the entropy or free energy of the system we must estimate the limiting structure from a simple potential energy minimization procedure.

We assume that this limit structure is very close to the structure of the string phase simulated at high but finite shear rates. We can thus utilize the minimum energy structure of the string phase in constructing our simulation box. (This assumption is mandatory because to determine the most stable structure of a string phase using simulations is impossible for both theoretical and practical reasons. First, there is no accepted thermodynamics for far-from-equilibrium systems; second, at very high shear rates the numerical stability of the algorithm requires very small time steps, even though the structural changes are extremely slow.) By this assumption, we hope to remove the familiar problem of equilibrium phase transitions: the disorder-order transition cannot be simulated sensibly if the symmetry of the small system hinders the formation of the ordered phase.

We use a simple approach in searching for the minimum energy arrangement. The first step is to select reasonable candidates as initial structures for an iterative procedure. The selection of initial structures is based on trivial and obvious symmetry and packing principles. The iterative procedure identifies the minimum energy structure in the neighborhood of the starting arrangement.

In Sec. II, we describe in detail the scheme given above and present the limit structure of the string phase for particles interacting with spherically symmetric short-ranged potentials. In Sec. III, we report NEMD simulations carried out by the Sllod algorithm [1] (so named because of its close relationship to the Dolls tensor algorithm) for a simple shearing liquid. Our study is only focused on the characteristics of the liquid-string transition. Emphasis is placed on the role of periodic boundary symmetry in the fluid-string transition. Recently, an entire phase diagram has been calculated for charge-stabilized colloidal suspensions by Stevens and Robbins [5]. Although their system is different from ours, we make comparisons with their results relevant to the present work. We also reproduce simulations of Yamada and Nosé [10] in order to explain the remarkable directional dependence of the stability of the string phase found by them. In the second part of Sec. III we investigate the number dependence of the transition in terms of simple phase variables. We calculate energy fluctuations moving along the transition path. We also calculate the so-called phase space compression factor [1]. Recently, this quantity was found to exhibit a local extremum property even far from equilibrium—at least approximately [11]. It can be considered to be an extension of the minimum entropy production principle [12] to far-from-equilibrium situations. In the last section we conclude the results of this study.

II. SEARCHING FOR MINIMUM ENERGY STRING STRUCTURES

A. Symmetry considerations

We adopt the usual convention of computer simulations: the liquid flows in the x direction and the velocity gradient can be measured along the y axis. ($\gamma \equiv \partial u_x / \partial y$. Note that in our convention the shear rate is γ and not $d\gamma/dt$.) In the $\gamma \to \infty$ limit the randomness of the thermal motion is negligible. The particles are moving along straight lines parallel to the x axis. Their velocity is determined solely by their y coordinates. The y and z coordinates of the particles can change only if there is a net force component in the y or z direction. If this happens, particles collide which generates further collisions, thus increasing the energy of the system. Consequently, any arrangement must maintain a strict symmetry, keeping the forces in the y-z plane identically zero. (Obviously, if we prevent collisions we create an artificially nondissipative system with zero x-y momentum flux.)

To avoid collisions the particles form strings or channels within which each of them has identical y coordinate, i.e., streaming velocity. There is no reason to distinguish among these channels from the point of view of symmetry. Due to the nonlinear repulsive forces acting between particles, the more uniform the arrangement the smaller the interaction energy. (We restrict our analysis to particles interacting only with short-range repulsive forces.) The best arrangement for dense, spherically symmetric objects in two dimensions is a hexagonal lattice. If one looks at the y-z plane (i.e., at the distribution of the channel centers perpendicular to the streaming motion) it is reasonable to assume that these channel centers approximately form a hexagonal lattice in this plane. Initially it is impossible to tell whether this lattice is completely regular (has the highest possible symmetry) or is only close to that. The hexagon in the plane can have three principally different orientations. (See Fig. 1). The first (I) represents the general case, when the hexagon is

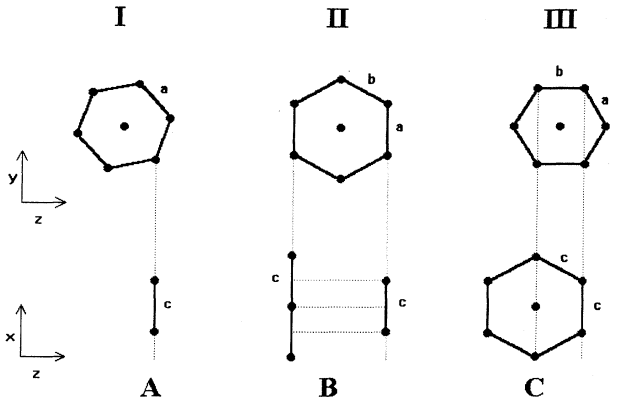

FIG. 1. Possible arrangements of particle channels (strings) projected onto the y-z plane (I, II, and III) and the corresponding x-z layers (A, B, and C).

arbitrarily oriented relative to the y or z axes. In the second case (II) a side of the hexagon is parallel to the y axis, while in the third case (III) a side is parallel to the z axis.

In case I none of the neighboring strings have identical y coordinates. Only particles in the same strings can have identical velocities. Particles in neighboring channels will pass by infinitely fast relative to one another. This means that in the y-z plane the arrangement should be a regular hexagon with distance a between adjacent strings. Let the interparticle distance within each channel (parallel to the x axis) be c. (See A in Fig. 1.) Clearly, at a given density a and c should have an optimum value when the energy of the arrangement is minimal.

Case II is quite similar to case I because particles having the same y coordinates are not adjacent neighbors. Nevertheless, for this arrangement we cannot assume a perfect hexagon in the y-z plane. One should distinguish two kinds of separations, a and b. As for the arrangement in the x-z plane it is easily recognized that the simple string structure of A can be replaced by B when the movement within channels of identical y coordinates is synchronized. (See Fig. 1).

The third hexagon orientation (III) is distinct from the previous two. The hexagon formed in the y-z plane need not be perfectly symmetric as in case I. However, the fact that adjacent channels have the same streaming velocity requires substantial synchronization in the x-z plane. The arrangement of the particles in the x-z plane must be as uniform as possible because the interatomic energies originating from particles with identical y values remain constant. This two-dimensional structure is shown in Fig. 1 as C. A perfect hexagon is formed in this plane with uniform distances c. Particles in neighboring strings are shifted by $c/2$ in the x direction relative to one another. For this structure $b=\sqrt{3}/2c$.

B. Results of the minimization procedure

The candidates described in the preceding section were used to build unit cells and then lattices from the cells. A simple program changed the x coordinates of the particles in a stepwise manner according to their y coordinates. This procedure mimicked the shearing motion of the system without defining the actual speed of the particles. The configurations obtained in this way represent consecutive snapshots of the system. Using periodic boundaries, we determined the potential energy for every configuration. We did this until the whole structure returned to its starting arrangement. We then averaged the configurational energy over snapshots of this whole period. Formally we can write this method as

$$U\approx\frac{1}{M}\sum_{k=1}^{M}\Phi_k(\mathbf{r}^N)=\frac{1}{M}\sum_{k=1}^{M}\sum_{i\neq j}^{N}\varphi(r_{ij}^{(k)})\ , \tag{1}$$

where M is the number of snapshots. φ is the spherically symmetric pair potential, N is the number of particles in the box,

$$\mathbf{r}_{ij}^{(k)}=[(x_i^{(k)}-x_j^{(k)})^2+(y_i-y_j)^2+(z_i-z_j)^2]^{1/2}\ ,$$

and $x_i^{(k)}=x_i^{(k-1)}+\Delta_i$ with $\Delta_i=\delta y_i$ where δ is a constant. In the limit of vanishing δ, Eq. (1) approaches the integral

$$U=\int_0^{S_{\max}}\Phi(\mathbf{r}^N(s))ds\ , \tag{2}$$

in which $x_i(s)=x_i(0)+sy_i$. The parameter $S_{\max}$ is the largest $s_{i,\max}$ value where the latter is defined as $s_{i,\max}y_i \bmod L=0$ and L is the edge length of the system.

Finally, we were searching for the minimum of the average potential energy (U) in terms of the a,b, and c structural parameters while keeping the density at a constant value. In principle, this minimization procedure can be performed analytically but due to the complexity of the resulting expression we opted for the simplest possible numerical technique. Since the time required for such calculations is small we mapped the energy values of the structures as functions of the a, b, and c parameters. We then chose smaller increments and performed refined calculations in the neighborhood of the a, b, and c values where the configuration energy per particle seemed to have a minimum. The accuracy of the method is determined by the number of discrete distance steps, i.e., grid size (δ), applied for generating the configurations.

The calculations were performed at four different densities, $\rho=0.9$, 1.0, 1.1, and 1.2. We applied three different repulsive potentials. The WCA potential is defined as $f(r)=4(r^{-12}-r^{-6})+1$ if $r<2^{1/6}$ and zero otherwise. The range of the soft sphere potential, $f(r)=r^{-12}$, is longer. The third potential is an exponential function: $f(r)=\exp[\kappa(1-r)]$ where $\kappa=10.0$. These potentials were chosen in order to give similar energy values. [If $r=1$ then $f(r)=1$ for all cases.] Their different behavior at longer ranges, however, can result in discrepancies originating mainly from second neighbor interactions. Here we used the usual reduced units of computer simulations [distances made dimensionless by dividing by the molecule diameter σ, energies made dimensionless by dividing by the characteristic interaction energy ε, number densities made dimensionless by multiplying by σ^3, strain rates made dimensionless by multiplying by $(m\sigma^2/\varepsilon)^{1/2}$, and times made dimensionless by

TABLE I. Properties of string unit cells at different densities using the WCA interaction model. [The accuracy of distances (a,c) and potential energy per particle (U/N) is one unit in the last shown digit.]

Structure		IA			IIIC	
Density	a	c	U/N	a	c	U/N
0.9	1.0807	1.0989	0.074 21	1.1224–1.1284	1.1265–1.1224	0.0
1.0	1.0425	1.0624	0.510 02	1.0687	1.0984	0.131 48
1.1	1.0102	1.0287	1.517 69	1.0301	1.0679	0.729 78
1.2	0.9816	0.9987	3.298 94	0.9986	1.0389	1.992 72

dividing by $(m\sigma^2/\varepsilon)^{1/2}$] [13].

In Table I we present the results for the case of the WCA potential. The advantage of this potential form is that there are no second neighbor interactions at these densities at all. In the case of the IA structure there are only two different distances a and c. The c value is always larger because in the x direction the distances stay constant during the motion, while a represents the distance between neighboring channels. Thus, a is the distance of closest approach of passing particles. Every particle has two neighbors at c (one in front and the other behind) and several others in the six adjacent channels. The IIB structure is not shown in the table because for the WCA potential $a=b$ and the whole arrangement is identical to the previous IA.

The comparison of the IIIC structure to IA shows that the packing of the former arrangement is preferred: the interatomic distances are larger so the energy per particle (U/N) is smaller at each density. For IIIC at $\rho=0.9$ there is no interaction energy at all if the a and c distances are within the range shown in the table. As the density increases, the interstring distance a shortens more rapidly than c, because in this structure every particle has six fixed neighbors.

Table II shows the same results as Table I for the case of the soft sphere interaction model. It is obvious that the resulting structural parameters are very similar to the results in the previous table, even though the energies are higher in this case due to the longer potential range. The IIIC model gives lower energies than the IA as in the case of the WCA potential. However, the differences are less pronounced.

The same results are shown in Table III for the case of exponential repulsion. The exponential repulsion provides very similar structural parameters with slightly higher energies than the r^{-12} repulsion. The IIIC arrangement again proves to be preferred over the IA structure. The IIB structure is not identical to the IA for the latter two potentials but the differences are so small in both structural parameters and energy that we also omitted them from Tables II and III. The decrease in energy as a result of changing from A to B in the x-z plane takes place in the fifth decimal digit. In fact, for $a=b$ this structure is slightly less favorable than IA because each particle interacts with more than two neighbors in the x-z plane. This reduced favorability is roughly compensated for by the split $b>a$, although the difference is again very small.

The final conclusion of this calculation is that the optimal structure is the IIIC arrangement. The basic characteristics of this structure have already been described in the case of colloidal systems [5,14] where this infinite shearing mechanism is inferred from the finite results. The strings form layers and these layers are sliding on each other. It is worthwhile to analyze this structure further. It is clear that the hexagonal arrangement in the x-z plane fills the space more uniformly than the A or B structure. Thus there is no point in considering IIIA or IIIB combinations. In Fig. 2 the x-z projection of the structure is shown. The circles mark the positions of particles and connecting lines emphasizing their hexagonal arrangement. Black circles form a plane while gray circles form another one above or below this plane. The distance between two neighboring planes is $\sqrt{3}a$. (Compare to Fig. 1.) The strings or channels are marked by lines parallel to the x axis.

The whole structure is only slightly different from the face centered cubic (fcc) or hexagonal closed packed (hcp) structures. In Fig. 3 we show two planes of these well-known structures. (The two lattices can only be distinguished by viewing the third plane.) It can be seen from the nonuniform $(\frac{1}{3}$-$\frac{2}{3})$ distribution of interchannel

TABLE II. Properties of string unit cells at different densities using the r^{-12} repulsion model. [The accuracy of distances (a,c) and potential energy per particle (U/N) is one unit in the last shown digit.]

Structure		IA			IIIC	
Density	a	c	U/N	a	c	U/N
0.9	1.082	1.096	1.2246	1.096	1.146	1.0817
1.0	1.045	1.058	1.8665	1.058	1.106	1.6487
1.1	1.012	1.028	2.7328	1.025	1.072	2.4138
1.2	0.983	0.995	3.8704	0.996	1.041	3.4187

TABLE III. Properties of string unit cells at different densities using the exponential interaction model. [The accuracy of distances (a,c) and potential energy per particle (U/N) is one unit in the last shown digit.]

Structure		IA			IIIC	
Density	a	c	U/N	a	c	U/N
0.9	1.083	1.094	1.4112	1.094	1.148	1.2720
1.0	1.046	1.056	2.0811	1.056	1.108	1.8906
1.1	1.013	1.023	2.9247	1.022	1.074	2.6748
1.2	0.985	0.992	3.9550	0.993	1.043	3.6380

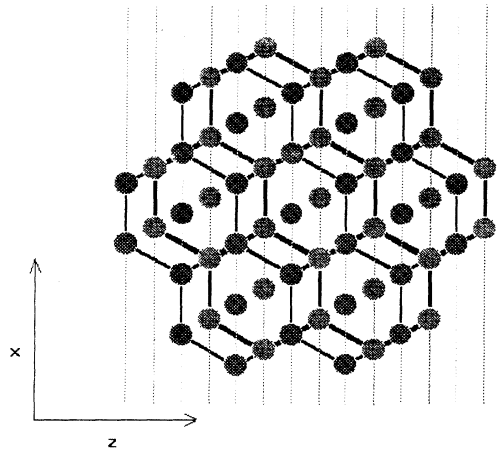

FIG. 2. Projection of two adjacent layers of the IIIC structure onto the x-z plane. Atoms of the two layers are distinguished by their shades. The thicker lines emphasize the hexagonal order in this plane. The thin lines represent paths of motion of particle strings in the x direction.

distances that this arrangement is less favorable than the IIIC. In Table IV we present the closest distances and the potential energies for the equilibrium fcc and hcp lattices at different densities. Comparing them to the properties of the IIIC structure under shear we can see the inevitable energy increase caused by the streaming motion of the particles.

We can relate the IIIC structure which is the minimum energy structure of the string phase of one-component spherical particles to its equilibrium minimum energy structure, the fcc or hcp lattice. In the latter cases the second (say, upper) layer of particles is formed by positioning each of them in the middle of neighboring particle triangles in the lower layer. In such a manner every second possible tetrahedron is built up. In the IIIC structure the particles of the upper layer are placed in the middle point of lines connecting particle neighbors in the first layer. The x position of these particles, however, is changing continuously. Thus, the arrangement shown in Fig. 2 is only momentarily the case.

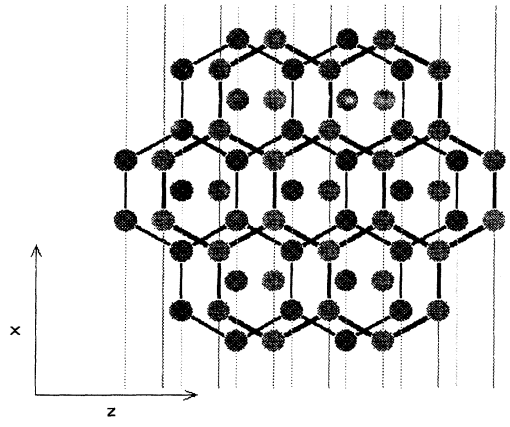

FIG. 3. The same as Fig. 2 for close-packed equilibrium structures. The hcp and the fcc lattices could be distinguished only by showing the third layer of the arrangements.

Taking into account the shift between adjacent particle layers described above the x, y, and z directions of the IIIC structure correspond to the $[\bar{1}10]$, $[111]$, and $[\frac{\bar{1}}{2}\frac{\bar{1}}{2}1]$ fcc directions, respectively. Finally in Fig. 4 we show the y-z plane of the IIIC structure. Different shades distinguish between particles in different y-z planes. As is evident, there are only second neighbors in the same y-z plane.

III. THE FLUID-STRING PHASE TRANSITION IN Sllod SIMULATIONS

A. Properties of the coexistence region in terms of periodic boundary symmetry

Having determined the limit structure of the string phase it is intriguing to compare it to structures realized in NEMD simulations. These structures are observed at finite T and γ which means that they would not be expected to reproduce our limit structure perfectly. Studying simulated string arrangements is much more difficult due to the constantly changing positions. One must attempt to grasp the characteristics of the systematic, synchronized collective motion of particles. A simple but reasonably informative way to do this is to monitor the projections of coordinates in the y-z plane.

To spare further computational complications in this work we used the Sllod algorithm in its simplest, standard PBT version [1]. This means that the formation of strings is preferred in the course of our simulations, so we cannot reach any conclusion which would support the claim of the possible string formation in real systems. The equations of motion for particle i are the following:

$$\dot{\mathbf{q}}_i=\frac{\mathbf{p}_i}{m}+\mathbf{i}\gamma y_i \ ,$$
$$\dot{\mathbf{p}}_i=\mathbf{F}_i-\mathbf{i}\gamma p_{yi}-\alpha\mathbf{p}_i \ , \tag{3}$$

where $\mathbf{p}$, $\mathbf{q}$, and $\mathbf{F}$ are the momenta, positions, and forces acting on particle i. $\mathbf{i}$ is a unit vector in the x direction and α is the thermostatting feedback multiplier. The value of the multiplier is determined through the Nosé-Hoover integral feedback method [13]

$$\dot{\alpha}=\frac{1}{Q}\left[\frac{T}{T_0}-1\right] , \tag{4}$$

where the temperature $T\equiv(1/3Nkm)\sum_{i=1}^{N}p_i^2$ and T_0 is its preset value. Q is the fictitious mass of the heat reservoir.

Stevens and Robbins have performed extensive calculations to determine phase diagrams for systems with a different kind of potential modeling charge-stabilized colloidal suspensions [5]. They applied both PBT and a version of PUT thermostats. [Since the shear rate has units of frequency it would be convenient to replace γ with a dimensionless quantity, the so-called Deborah number (De). The Deborah number is defined as a product of the shear rate and a characteristic relaxation time of the sys-

TABLE IV. Energy per particle (U/N) for close-packed structures (no shear present). In the case of the WCA interaction there is no energy difference between the fcc and hcp structures.

ρ	Closest distance	U/N WCA	U/N $(1/r)^{12}$ fcc	U/N $(1/r)^{12}$ hcp	U/N exp. fcc	U/N exp. hcp
0.9	1.162 58	0.0	0.9938	0.9943	1.1856	1.1857
1.0	1.122 46	0.0	1.5148	1.5155	1.7723	1.7725
1.1	1.087 36	0.2646	2.2178	2.2188	2.5197	2.5200
1.2	1.056 28	1.1616	3.1410	3.1425	3.4414	3.4419

tem. However, since there is no unique convention for the choice of the relaxation time we retain the shear rate as the independent variable.] Their nonequilibrium phase diagram showed regions of ordered and disordered (liquid) phases of colloids as functions of De and ρ_s. The latter symbol represents the concentration of the added salt which screens the Coulomb repulsion between the colloids. These independent variables were chosen in order to facilitate the comparison with experiments.

Stevens and Robbins [5] paid particular attention to the equilibrium solid-shear melted liquid region. To determine the coexistence curve they formed an interface of the two phases before starting the simulation. The interface was created on the surface of the equilibrium crystal of colloid particles. Our understanding of their paper is that they determined the liquid-string ("reentrant solid") line in the same way ("two-phase method") as that of the equilibrium crystal-shearing liquid curve. They found a very narrow coexistence region for this transition using 864 or 768 particles.

Shear melting was out of the scope of our present study because we are interested only in the upper part of the phase diagram: the fluid-string transition region. We employed an alternative way of removing the distorting effects caused by the small system size applied in computer simulations. We assumed—analogously to fluid-solid phase transitions in equilibrium simulations—that the ordering direction of the process is hindered much more than the reverse transition. This gives rise to a pronounced hysteresis as we alluded to earlier. In order to decrease this effect we determined the transition line starting from high-shear-rate simulations at a given temperature. The system was formed by 512 particles having IIIC initial symmetry. Since this structure must be very close to the high-γ-limit arrangement for the string phase, we expect to decrease the asymmetry between the fluid→string and the string→fluid paths of the transition substantially. Clearly, the liquid phase is less sensitive to the chosen symmetry of periodic boundary conditions. All the calculations reported in the following have been performed in the same way. The symmetry of the simulation box is IIIC unless written otherwise. The time increment in the integration step varied from 0.001 to 0.004 in reduced units depending on T and γ.

In Fig. 5 we show a "phase diagram" calculated for WCA particles at $\rho=0.9$. The symbol X marks the equilibrium melting temperature which quickly decreases as the shear rate increases. (This effect can only be studied in simulations where the stress is the externally imposed independent variable but we omitted these calculations this time.) The area between the dotted and solid lines represents the coexistence region of liquid and string phases. Below this region the system forms an amorphous liquid (high-T, low-γ region), while above this region the system is ordered (high-γ, low-T region). We found—in contrast to the results of Stevens and Robbins [5]—a reasonably wide coexistence region. The upper limit of this region is marked—decreasing γ gradually at a given temperature and density—after the first irregular arrangement appeared in the sample. At the value of the lower boundary the ordered phase disappeared completely. The range of the coexistence region seems to widen with increasing γ.

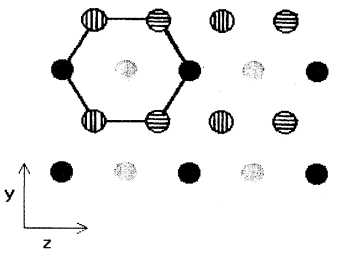

FIG. 4. The y-z projection of the IIIC structure. The different shades mark particles belonging to the same layer, i.e., having identical x coordinates instantaneously. Note that these relative positions change in the course of streaming.

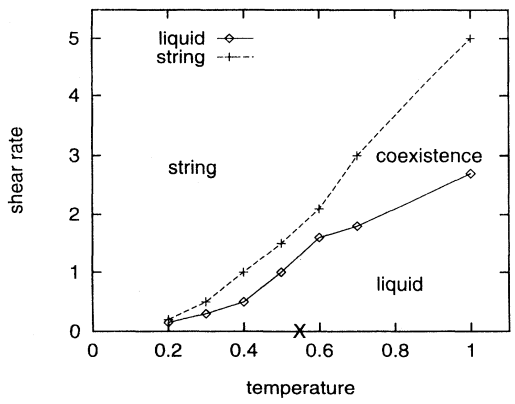

FIG. 5. Nonequilibrium "phase diagram" of a system consisting of 512 WCA particles, at a reduced number density $\rho=0.9$. A $\times$ marks the equilibrium melting point. (See text for definition of reduced quantities.)

It should be noted before moving on that the determination of an accurate phase diagram is a notoriously difficult matter even for equilibrium systems. Thus we cannot claim that Fig. 5 is "the phase diagram" of this "phase equilibrium." Obviously, the results are functions of the details of the simulations and the particular methods one uses to identify the phases.

In Fig. 6 we show snapshots of systems at the same temperature but different shear rates. These pictures were used to pinpoint transition lines of the phase diagram shown in the Fig. 5. The circles represent particles projected onto the y-z plane. In Fig. 6(a) one can see the string channels where the particles are one on top of the other. If one compares this figure to Fig. 4 it is easy to identify the sixfold symmetry in the y-z plane. (The mechanism is more or less a layer-over-layer sliding motion.) The number of lattice defects is very small. In Fig. 6(b) the structure of the system in the coexistence region is visualized. The ratio of the area occupied by the string and the disordered phase is roughly proportional to the distance from the pure ordered or pure disordered phase in the phase diagram, as in first order equilibrium phase transitions. Figure 6(c) shows a disordered structure, close to the phase transition. In all three cases the temperature was unity, the reduced number density $\rho=0.9$, and the shear rates in Figs. 6(a), 6(b), and 6(c) were 7.0, 2.8, and 2.5, respectively.

The coexistence of the fluid and string phases in the simulation box has already drawn the attention of Erpenbeck [2] and Yamada and Nosé [10]. They both found the interface between the phases to be parallel to both the flow direction and the velocity gradient. In our notation this corresponds to the x-y plane. A snapshot of particles in the y-z plane by Evans *et al.* [4] supports this finding.

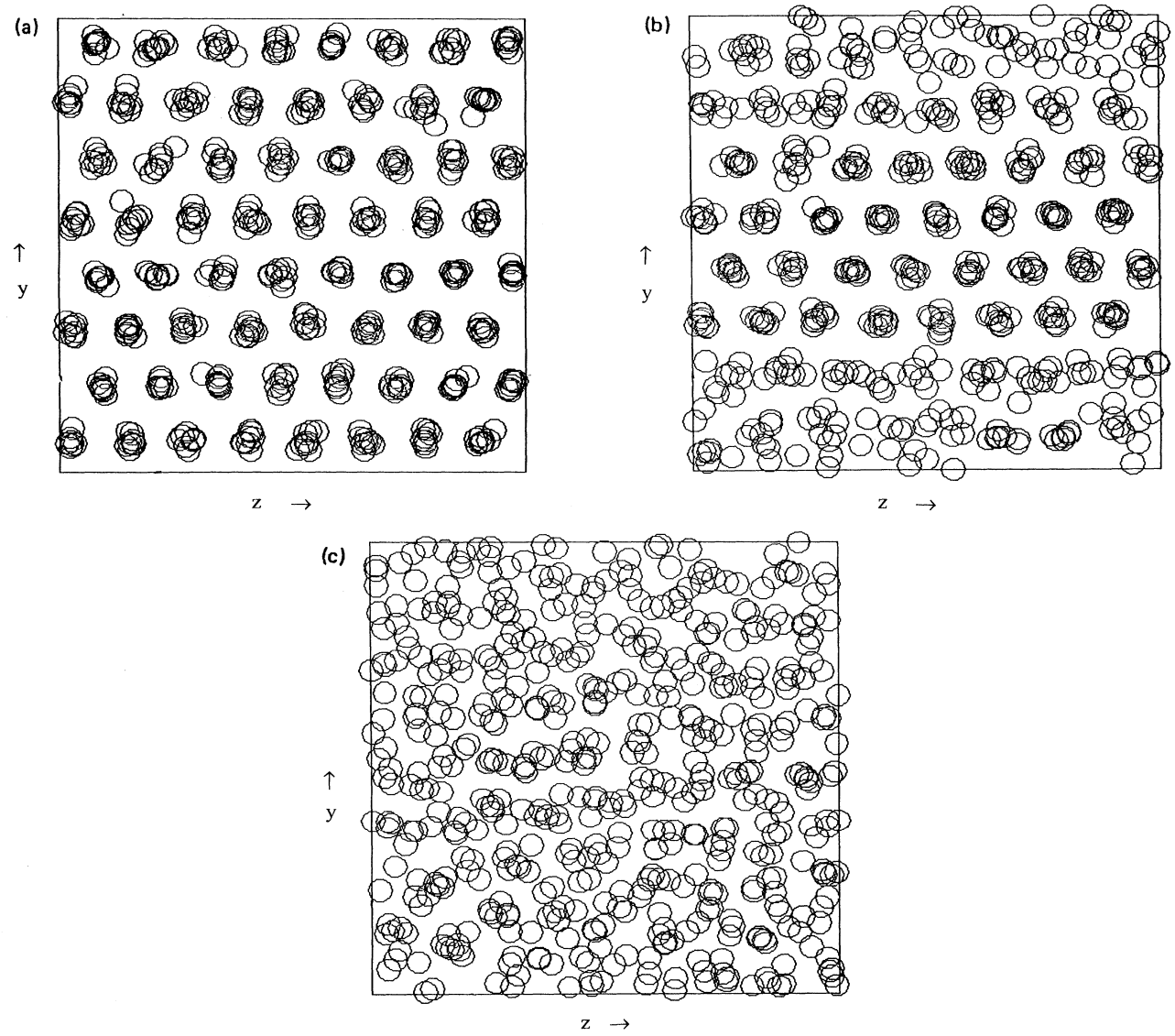

FIG. 6. Snapshots of simulated particle arrangements projected onto the y-z plane, at $T=1.0$, $\rho=0.9$, and (a) $\gamma=7.0$; (b) $\gamma=2.8$; (c) $\gamma=2.5$. (See text for definition of reduced units).

However, none of these authors have considered the geometry of the simulation cell and the effect of its variation.

We considered the same system studied by Yamada and Nosé [10], except for the exact form of the interaction potential. We used the WCA rather than the usual Lennard-Jones potential with a cutoff at $r=2.9$. We chose the same number density, temperature, and shear rate: $\rho=0.8174$, $T=0.71$, and $\gamma=2.42$, respectively, all in reduced units. We confirmed from our simulations that at this point of the phase diagram the fluid and string phases coexist. However, we also found that the effect of the cell geometry on the structure is substantial.

We performed simulations with three different cell geometries. The first was the one corresponding to the III*C* structure which has been found to be optimal in the infinite-shear-rate limit (see Sec. II). This time we omitted the slight differences resulting from the minimization procedure. The relative box lengths in the x, y, and z directions, L_x, L_y, and L_z, were 1, $\sqrt{3}/2$, and $\sqrt{3}/2$, respectively. Our second simulation box was one corresponding to the fcc lattice geometry with its two-dimensional close-packed layers in the x-z plane. The x, y, and z directions of the box correspond to the $[\bar{1}10]$, and $[111]$, and $[\frac{\bar{1}}{2}\frac{\bar{1}}{2}1]$ fcc directions, respectively. The corresponding relative box lengths were 1, $\sqrt{2}/\sqrt{3}$, and $\sqrt{3}/2$. The third simulation box considered was a simple cube.

All these simulations were started from an equilibrium liquid structure. The reason for this was not to bias any of the initial box symmetries. The time increment in the integration was 0.001. In the first two cases the number of particles was 1728 whereas in the cubic box it was 1372. The runs were continued until the structure of the system reached a steady state. In Fig. 7 we present snapshots of the simulation boxes, where the positions of all the particles (represented by small circles) are projected onto the y-z plane. The pictures clearly illustrate the difference between the results. Different simulation boxes at the same density, temperature, and shear rate result in structurally and energetically different phases.

In Fig. 7(a) one can see the coexistence of the ordered and disordered phases, but the phase boundary is perpendicular to the orientation found by Yamada and Nosé [10]. The orientation of the phase boundary shown in Fig. 7(a) was consistently found in our simulations when the III*C* box geometry was used. In the next shapshot [Fig. 7(b)] a different pattern of the string phase can be seen, coexisting with the fluid phase. The string phase has a clearly visible hexagonal symmetry, which is caused by the shape of the simulation box. The orientation of the phase boundary, however, seems to be parallel to the velocity gradient, which was found by Yamada and Nosé [10]. They have shown that this structure is more favored than that rotated by 90° along the x axis. In light of our results, we believe this is simply due to the fact that the string phase favors the III structure [as defined in the preceding section (see Fig. 1)] as opposed to the I or II ones and this III→II change is the most important effect the 90° rotation has, since the liquid phase is isotropic. In Fig. 7(c) we present a snapshot of the cubic simulation box. There is no string phase present, only some vague ordering relative to an equilibrium liquid. In Table V we collected some features of the three simulations with different box symmetries.

B. Number dependence of the phase transition

We experienced that the structure of the string phase and the properties of the transition strongly depend on the symmetry imposed upon our model by the periodic boundary conditions of the simulations. At this stage there is another important question to be decided: what is the number dependence of the transition? To obtain sensible answers from a limited computation we must narrow the scope of our study. In the following we report on simulations carried out only with the III*C* periodic boundary symmetry. We believe that the other usual shapes of the simulation box have little relevance to our original question: What is the possibility of this transition taking place in real shearing fluids? In addition to following the structural details of the system by coordinate projections we monitored some simple phase variables showing drastic changes in this region.

The pressure and the viscosity as functions of shear rate at a given temperature are clearly indicating the phase transition. (See Fig. 8.) Nevertheless, it is quite difficult to decide in the course of the simulation whether the actual state of the system is pure shearing fluid or ordered string or their mixture of some ratio.

At equilibrium the second derivatives of thermodynamic potential functions, the heat capacities in particular, are sensitive indicators of phase transitions. It is a standard exercise in equilibrium statistical mechanics to show that the isochoric heat capacity c_v is proportional to internal energy fluctuations, while the isobaric heat capacity c_p is related to enthalpy fluctuations. Due to the probable split of the thermodynamic and kinetic temperature for NESS systems these simple equilibrium relationships break down [15–18]. Heat capacities can be derived using the Kawasaki distribution or transient time correlation function formalism if one is interested in the change of internal energy with respect to a change in the kinetic temperature [1]. The resulting Kawasaki expression contains two terms. The first is simply the steady state energy fluctuation which is larger in NESS systems than in equilibrium. The contribution of the second term, however, more than compensates for the increase in internal energy fluctuations. Thus the isochoric heat capacity turns out to be smaller in NESS systems than in equilibrium [1].

The second term of this heat capacity expression is a time correlation function which is difficult to evaluate. On the other hand, we do not know how this expression is related to NESS phase transitions. Therefore we calculated only the internal energy fluctuations as functions of the external field. In Fig. 9 the internal energy fluctuations per particle are shown for the $T=0.5$, $\rho=0.9$ system. The system forms a crystalline solid at equilibrium. The upper border of the fluid-string coexistence region is around $\gamma=1.5$. (See Fig. 5.) At this shear rate the calculated energy fluctuations exhibit a much larger value than

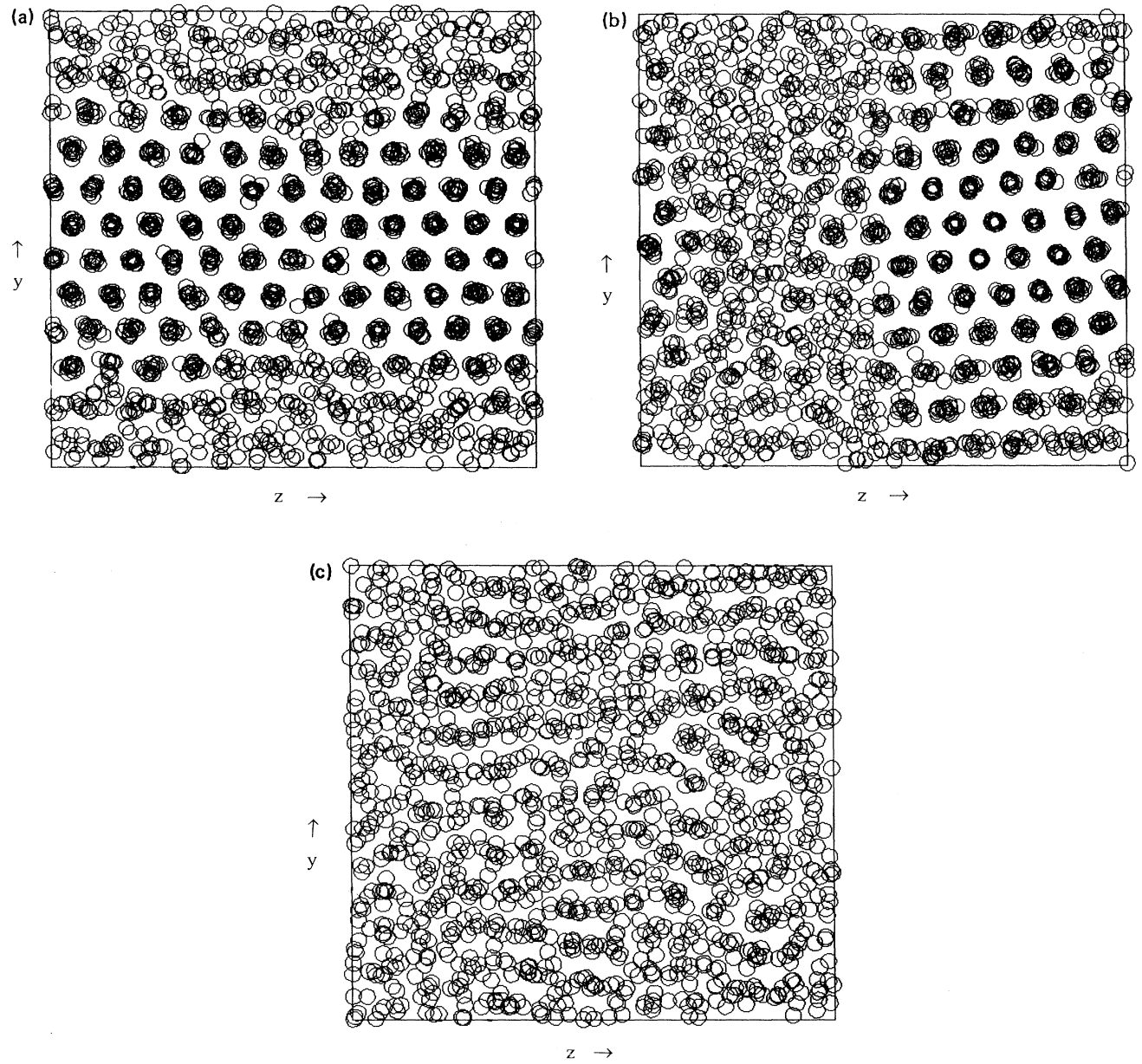

FIG. 7. (a) Snapshot of a simulated system projected onto the y-z plane, at $T=0.71$, $\rho=0.8174$, $\gamma=2.42$, and $N=1728$. The shape of the simulation box was that of the unoptimized IIIC unit cell. (b) The same as for (a), but the shape of the box was that of the fcc unit cell with its two-dimensional close-packed layers in the x-z plane. (c) The same as in (a) and (b), but the simulation cell was cubic, and the number of particles was 1372. (See text for definition of reduced units.)

either in the amorphous fluid phase or in the string phase. This is the point where the amorphous structure appeared when we moved from high-shear systems to low-shear ones. The shape of the curve is reminiscent of first order phase transitions between equilibrium phases. This behavior seems to be in accordance with the overall characteristics of the fluid-string transition.

An even more promising quantity to study may be the so-called phase space compression factor [1]. Recently, Evans and Baranyai (EB) proposed a variational principle

TABLE V. Results of the three simulations of different periodic boundary conditions. (All the quantities are given in reduced units.)

Cell shape	IIIC	fcc	Cubic
Pressure	5.65	6.21	7.71
(Energy)/N	1.74	1.83	2.08
Stress	1.59	1.94	3.09
(Energy fluctuation)/N	1.02	1.51	1.78

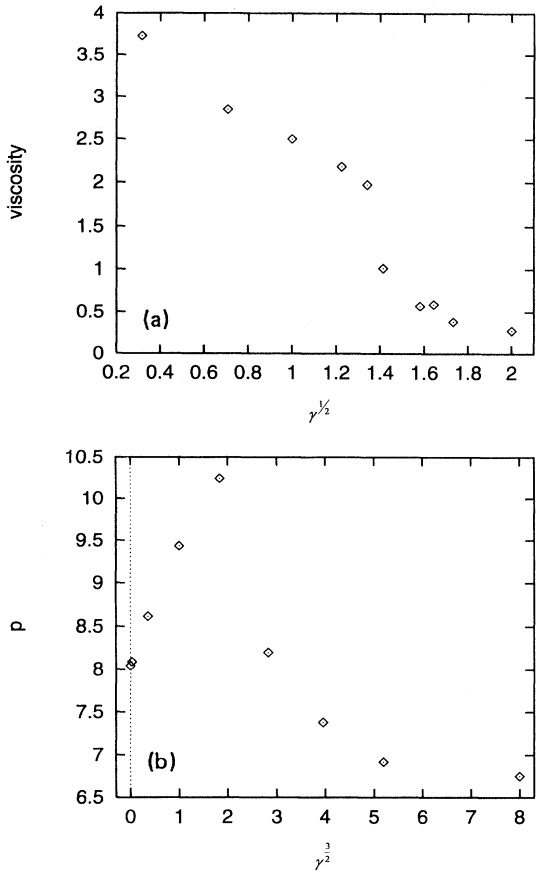

FIG. 8. (a) Shear viscosity plotted against $\gamma^{1/2}$ for a $T=0.5$, $\rho=0.9$, and $N=512$ system. (b) The hydrostatic pressure $p=\frac{1}{3}\mathrm{Tr}(\mathbf{P})$ is plotted against $\gamma^{3/2}$ for the same system.

for nonequilibrium steady state systems [11]. They assumed that under constant internal energy E, volume V, and particle number N conditions the average of the phase space compression factor $\langle \Lambda \rangle$ is a local maximum in terms of endogenous variables of the system. According to their definition endogenous variables are phase variables which are not external parameters or generalized thermodynamic forces (e.g., shear rate) of fluxes conjugate to these fixed forces. These variables are solely functions of $\Gamma \equiv (\mathbf{p}_1, \mathbf{p}_2, \ldots, \mathbf{p}_N, \mathbf{q}_1, \mathbf{q}_2, \ldots, \mathbf{q}_N)$. The phase space compression factor is defined by the Liouville equation

$$\Lambda(\Gamma,t) \equiv -\frac{d\ln f(\Gamma,t)}{dt} , \tag{5}$$

where $f(\Gamma,t)$ is the probability density of the NESS system in phase space and Γ represents a point in phase space.

The principle has not been proven rigorously but the authors provided numerical evidence from NEMD simulations [11]. Since then these numerical findings have been supported by an approximate solution of the Boltzmann equation [19]. It appears that the proposed principle must be valid, at least approximately, for NESS systems far beyond the linear irreversible regime.

This variational principle can be viewed as a nonlinear generalization of the well-known minimum entropy production principle of linear irreversible thermodynamics [12], because close to equilibrium the two statements are identical. Far from equilibrium, however, the generalized statement bypass the ambiguities of entropy or entropy production definitions because the phase space compression factor is a simple, microscopic phase variable. It is easy to show that the phase space compression factor is closely related to the thermostatting multiplicator [1]. For Sllod dynamics

$$\Lambda(\Gamma) = -3N\alpha(\Gamma) + o(1) . \tag{6}$$

The second term on the right-hand side of (6) represents order 1 differences depending on the exact number of degrees of freedom.

The global behavior of the proposed extremum principle, however, has not been tested yet. The shearing liquid-string phase transition provides a good opportunity to do so at least from the liquid side of the transition where the instability of the amorphous liquid system is beyond doubt in PBT Sllod dynamics. In Fig. 10(a) we show $-\langle \Lambda \rangle / N$ (solid line) as a function of shear rate at $E/N=1.0$, $N=512$, and $\rho=0.9$. $-\langle \Lambda \rangle / N$ quickly increases with γ. Then at the coexistence region there is a local minimum before it increases further in the string regime.

The quantity $\langle \Lambda \rangle / N$ could be used as a variable having extremum properties globally if and only if the two curves corresponding to the two regimes join at the same value in the coexistence region. Obviously, this is not the case. However, we assume a strong number dependence in the coexistence region so we calculated the same curves for different system sizes ($N=512$, 1200, and 1728). These results can also be seen in Fig. 10(a). Our assumption was completely justified: the phase space compressibility factor behaves markedly differently for different system sizes. (We note again that these calculations were also done with IIIC simulation box symmetry.)

There are two universal curves which have been marked by arrows. [See both Figs. 10(a) and 10(b).] The first is the liquid curve which is identical for all three simulations irrespective of system size. We also identified

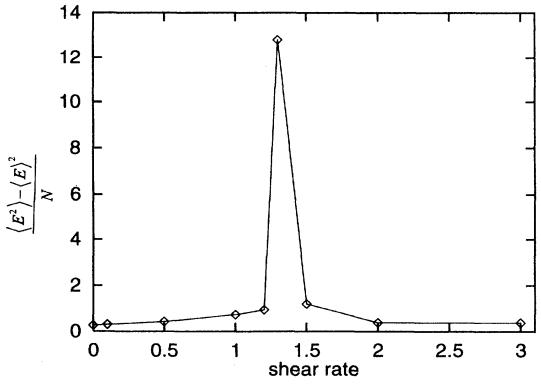

FIG. 9. Internal energy fluctuations of the system ($N=512$, $T=0.5$, and $\rho=0.9$) as functions of the shear rate.

a unique (number independent) string line but a reasonable fit to this curve by simulation data could only be achieved by small systems. (Data for smaller than 512 particle systems are not shown in the figure.) There are differences in the transition region. In the case of the $N=512$ system $-\langle\Lambda\rangle/N$ falls off vertically from the liquid curve to the string line. Basically, there is no coexistence region at all. The larger the system the smaller the gap between the liquid and the string curves while the coexistence region increases. This is quite evident from the $-\langle\Lambda\rangle/N$ values of the largest system. In fact, we could not obtain pure strings for this system at all in the reported shear-rate range. We performed some pilot calculations for even larger systems but we found the same result. The larger the system the more difficult to get the pure ordered string phase despite the favorable periodic boundary conditions and the profile biased thermostat.

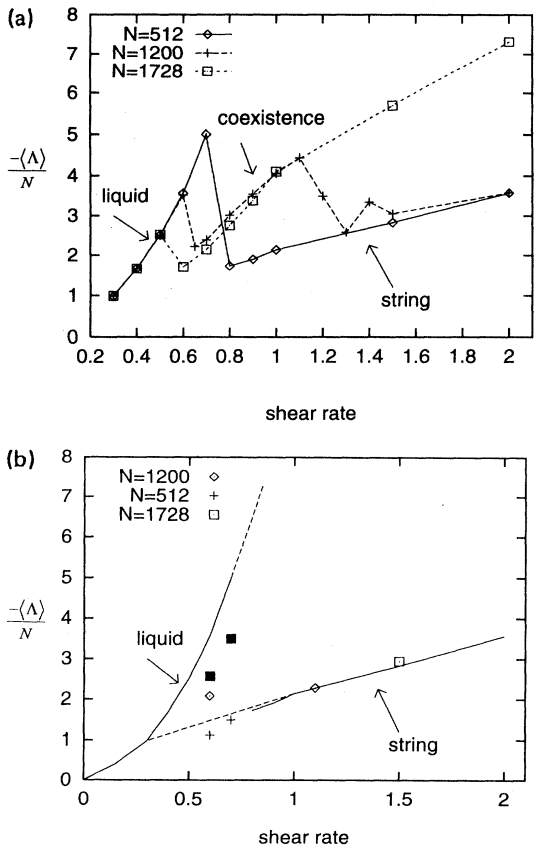

FIG. 10. (a) $-\langle\Lambda\rangle/N$ as a function of shear rate for three different system sizes. The symbols represent the results of the calculations. The uncertainty of these values is smaller than the symbols shown. All these simulations were performed using III*C* symmetry. (b) The same as (a) but the symbols of the simulation results shown in (a) are removed. Only the number independent liquid and string curves are shown. Dashed lines are extrapolations of these two (solid) curves to regions where we could not calculate $-\langle\Lambda\rangle/N$ directly. Open symbols represent additional calculations with biased, *y-z* thermostat stabilizing the string structure. Filled squares stand for simulations performed using the *x* thermostat, so stabilizing the disordered structure.

There is a very appealing explanation for the strong number dependence of the transition region on the disordered liquid side. To form an interface in a small system requires extra thermodynamic potential, whatever it might be for this far-from-equilibrium situation. This means that the pure shearing liquid phase is preferred to coexistence in small systems. As the number of particles increases the relative weight of the interface region gets smaller so the phase transition can happen at lower shear rates. In the thermodynamic limit one might expect the transition to take place where the extrapolated, number independent string line joins the liquid line. [See Fig. 10(b).] If this is so, the EB principle [11] is valid because the system opts for the smallest possible $-\langle\Lambda\rangle/N$ value.

However, the behavior of the system at higher shear rates is in contradiction with the EB principle. As the system gets larger, the coexisting liquid and string phase becomes preferred to the pure string. In the case of 1728 particles we could not get pure string phases in the shear-rate range studied. Since the phase space compression factor's value of strings is considerably lower than that of the coexistence phase this behavior does not comply with the extremum principle.

To eliminate possible problems related to the metastable character of the string phase we performed several calculations with special thermostats. In the string phase the particles have most of their kinetic energy (random impulses) in the *x* direction. Designing the thermostatting procedure in such a way that while keeping the energy of the system fixed we remove kinetic energy only from the *x* direction we destabilize the string and help the disordered liquid to be formed [20]. Doing this inversely and removing the energy only from the *y* and *z* directions stabilizes the ordered phase.

In Fig. 10(b) we compare the curves of phase space compressibility values with symbols originating from the biased thermostat simulations. The universal liquid and string curves are represented by solid lines. The dashed lines are their extrapolations to regions we could not calculate directly. The crossing of these two curves might mark the transition *in the thermodynamic limit* that we alluded to earlier. Open symbols show results when the string phase was stabilized (*y-z* thermostats) and filled squares refer to the opposite (*x* thermostat) when the string phase was destabilized. In the $N=1728$ system the *x* thermostat increases the shearing liquid part of the coexistence phases but is not able to remove the strings completely. Nevertheless, the higher phase space compressibility is in accordance with the EB principle [20].

As can be seen the *y-z* thermostat removes the liquid part from the system of coexisting phases. The resulting phase space compressibility factor gets onto the universal string line. In the case of the small system it enables us to extend the string region towards lower shear rates. These results are in contradiction with the studies of Evans and Baranyai [20] where the partial thermostats provided higher $-\langle\Lambda\rangle/N$ values. To see that the stability of the coexistence is not accidental, after a run with the *y-z* thermostat we changed back to the normal *x-y-z*

Gaussian thermostat. The pure string system returned to the coexistence phase, which indicates that under these conditions the coexistence phase is more stable than the string.

It seems that as the system becomes larger the stability of the pure string phase tends to be reduced relative to that of the coexisting phase. In the thermodynamic limit we may not obtain strings at all even in the artificial PBT Sllod system.

IV. CONCLUSIONS

We studied the amorphous liquid→string phase transition taking place in strongly shearing Sllod model systems in order to evaluate the possibility of such a transition taking place in real systems.

First, using an iterative procedure, we identified the most stable arrangement in the high-density, infinite-shear-rate limit for several short-ranged repulsive potentials. We showed how this structure is related to close-packed equilibrium structures, are hcp and fcc lattices.

To avoid the problem of nonergodicity familiar from the simulations of equilibrium phase transitions, we applied this limit structure as the starting arrangement in the periodic system, thus stabilizing the string phase. A further justification of this approach was that we could explain certain structural peculiarities experienced by others simulating similar systems [10]. We studied the structural details of the transition in terms of periodic symmetry imposed upon the model system. We found that the symmetry constraints of the simulation manifested in the shape and the initial particle arrangement of the system box are extremely important and must be taken into account in similar studies.

Performing simulations with the special symmetry of the limit structure we experienced a much stronger tendency of the ordered and disordered phases to coexist than Stevens and Robbins did in their colloidal suspension model calculations [5]. The discrepancy can be attributed to several factors different in these model calculations. However, for large systems we experienced difficulties in simulating pure strings. These systems tend to form coexisting phases over a reasonably wide range of shear rates. Since both the profile biased synthetic thermostat and the special symmetry of the periodic arrangement prefer the string phase, we believe the string formation has an inherent instability. In light of these results, we believe that calculations where stable "reentrant solid" phases were found [5] should also be performed on different (possibly very large) systems using different box symmetries to see how these factors influence the properties of their model system.

We also studied the number dependence of the liquid-string transition in terms of the so-called phase space compressibility factor. We found that this quantity might correctly indicate the decreasing stability of the (PBT Sllod) shearing liquid phase in the thermodynamic limit as the shear rate increases. Since the stability of the string phase in this limit seemed to diminish we could not reach definitive conclusions about the higher-shear-rate behavior of the phase space compressibility factor.

ACKNOWLEDGMENTS

A. B. acknowledges the financial support of OTKA Grant No. F7218 and is indebted to Professor Peter T. Cummings for his helpful comments and advice.

[1] D. J. Evans and G. P. Morriss, *Statistical Mechanics of Nonequilibrium Liquids* (Academic, New York, 1990).
[2] J. J. Erpenbeck, Phys. Rev. Lett. **52**, 1333 (1984).
[3] B. J. Ackerson, Physica **174**, 15 (1991).
[4] D. J. Evans, S. T. Cui, H. J. M. Hanley, and G. C. Straty, Phys. Rev. A **46**, 6731 (1992).
[5] M. J. Stevens and M. O. Robbins, Phys. Rev. E **48**, 3778 (1993).
[6] B. J. Ackerson and P. N. Pusey, Phys. Rev. Lett. **61**, 1033 (1988).
[7] S. Y. Liem, D. Brown, and H. R. Clarke, Phys. Rev. A **45**, 3706 (1992).
[8] W. Loose and S. Hess, in *Microscopic Simulations of Complex Flows*, edited by M. Mareschal (Plenum, New York, 1990); W. Loose and G. Ciccotti, Phys. Rev. A **45**, 3859 (1992).
[9] D. J. Evans, Phys. Rev. A **25**, 2788 (1982).
[10] T. Yamada and S. Nosé, Phys. Rev. A **42**, 6282 (1990).
[11] D. J. Evans and A. Baranyai, Phys. Rev. Lett. **67**, 2597 (1991).
[12] S. R. De Groot and P. Mazur, *Non-Equilibrium Thermodynamics* (Dover, New York, 1984).
[13] M. P. Allen and D. Tildesley, *Computer Simulation of Liquids* (Oxford University Press, Oxford, 1987).
[14] B. J. Ackerson, J. B. Hayter, N. A. Clark, and L. Cotter, J. Chem. Phys. **84**, 2344 (1986).
[15] D. J. Evans, J. Stat. Phys. **57**, 745 (1989).
[16] A. Baranyai, D. J. Evans, and P. J. Daivis, Phys. Rev. A **46**, 7593 (1992).
[17] A. Baranyai and D. J. Evans, Mol. Phys. **74**, 353 (1991).
[18] J. Casas-Vázquez and D. Jou, Phys. Rev. E **49**, 1040 (1994).
[19] J. J. Brey, A. Santos, and V. Garzó, Phys. Rev. Lett. **70**, 2730 (1993).
[20] D. J. Evans and A. Baranyai, Mol. Phys. **77**, 1209 (1992).